Supplement of

Divergent Land and Ocean Biome Trajectories in a Warming World

Debashis Paul[1], Eun-Jin Park[2], Eun Young Kwon[1,2], Sharif Jahfer[1], Sahil Sharma[1], M.G. Sreeush[3]

[1]Center for Climate Physics, Institute for Basic Science (IBS), Busan, Republic of Korea
[2]School of Carbon Neutrality and Climate Change, Pusan National University, Busan, Republic of Korea
[3]Alfred-Wegener-Institut, Helmholtz-Zentrum für Polar- und Meeresforschung, Bremerhaven, Germany

Correspondence to: Eun Young Kwon (ekwon957@gmail.com)

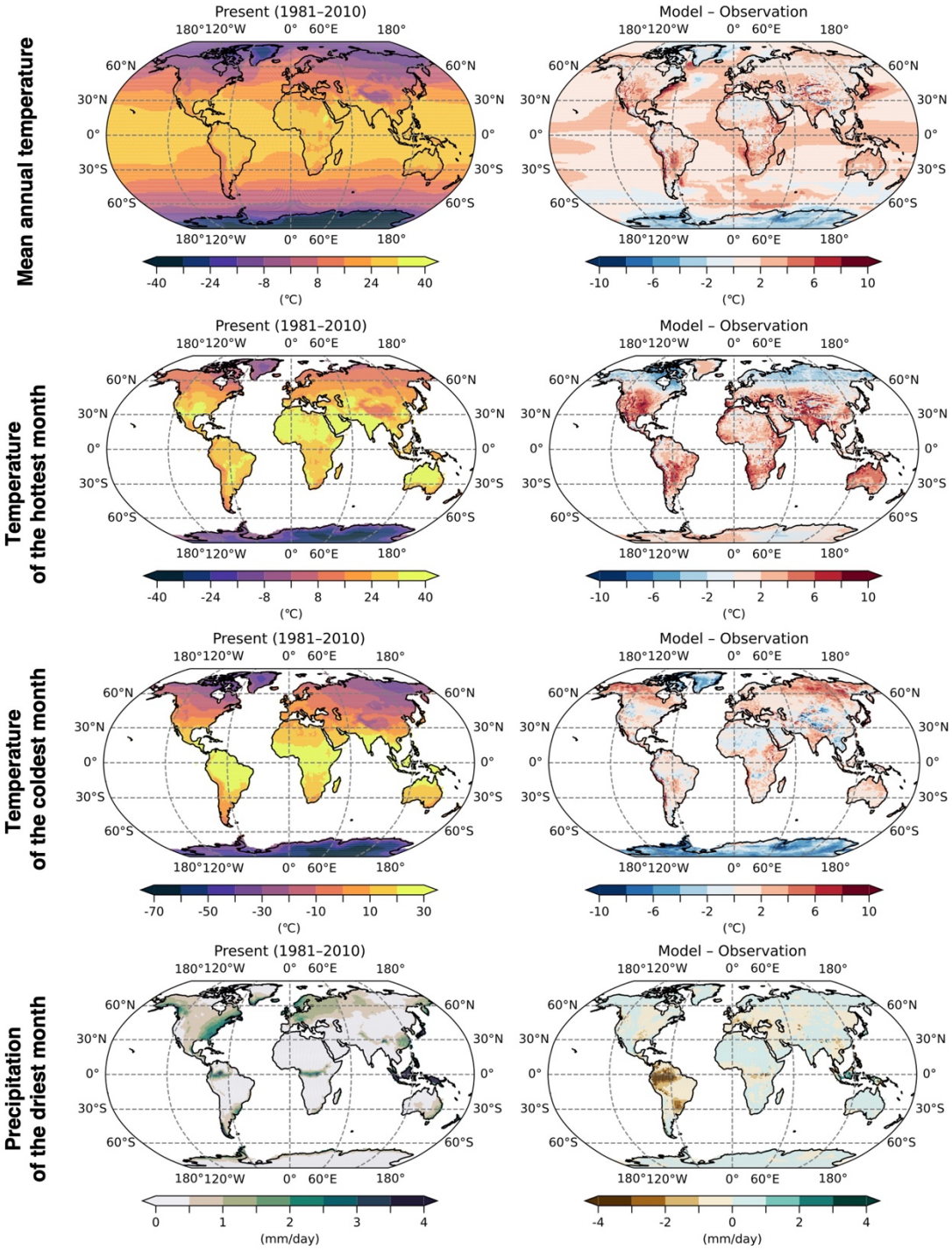

Figure S1. Simulated present-day (1981–2010) distributions of key climatic variables and their comparison with observed climatology. Rows show (top) mean annual temperature (°C), (second) temperature of the hottest month (°C), (third) temperature of the coldest month (°C), and (bottom) precipitation in the driest month (mm/day). The left column displays the simulated climatology for 1981–2010, and the right column shows the model bias (i.e., model minus observation).

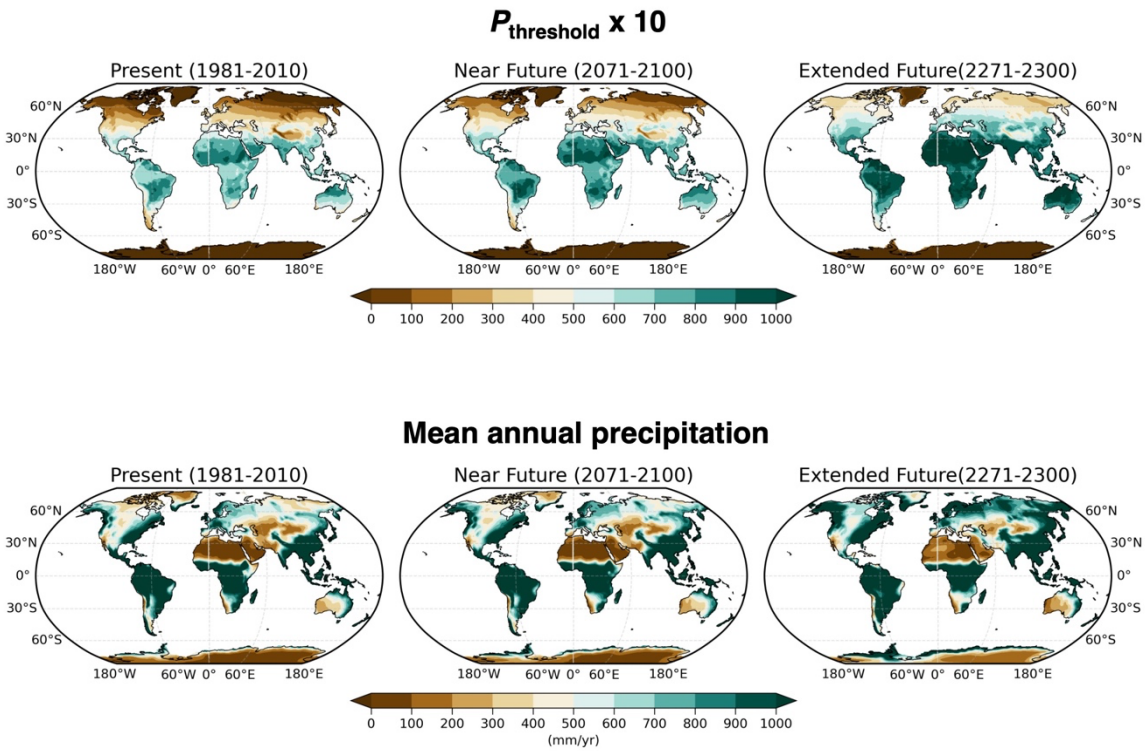

Figure S2. Aridity threshold and mean annual precipitation used in the Köppen-Geiger classification. Maps display global patterns of (top row) the precipitation threshold ($P_{threshold}$×10) and (bottom row) mean annual precipitation in mm/yr. Columns from left to right represent the present (1981–2010), near future (2071–2100), and extended future (2271–2300) periods. Regions where mean annual precipitation falls below the precipitation threshold are classified as arid climates.

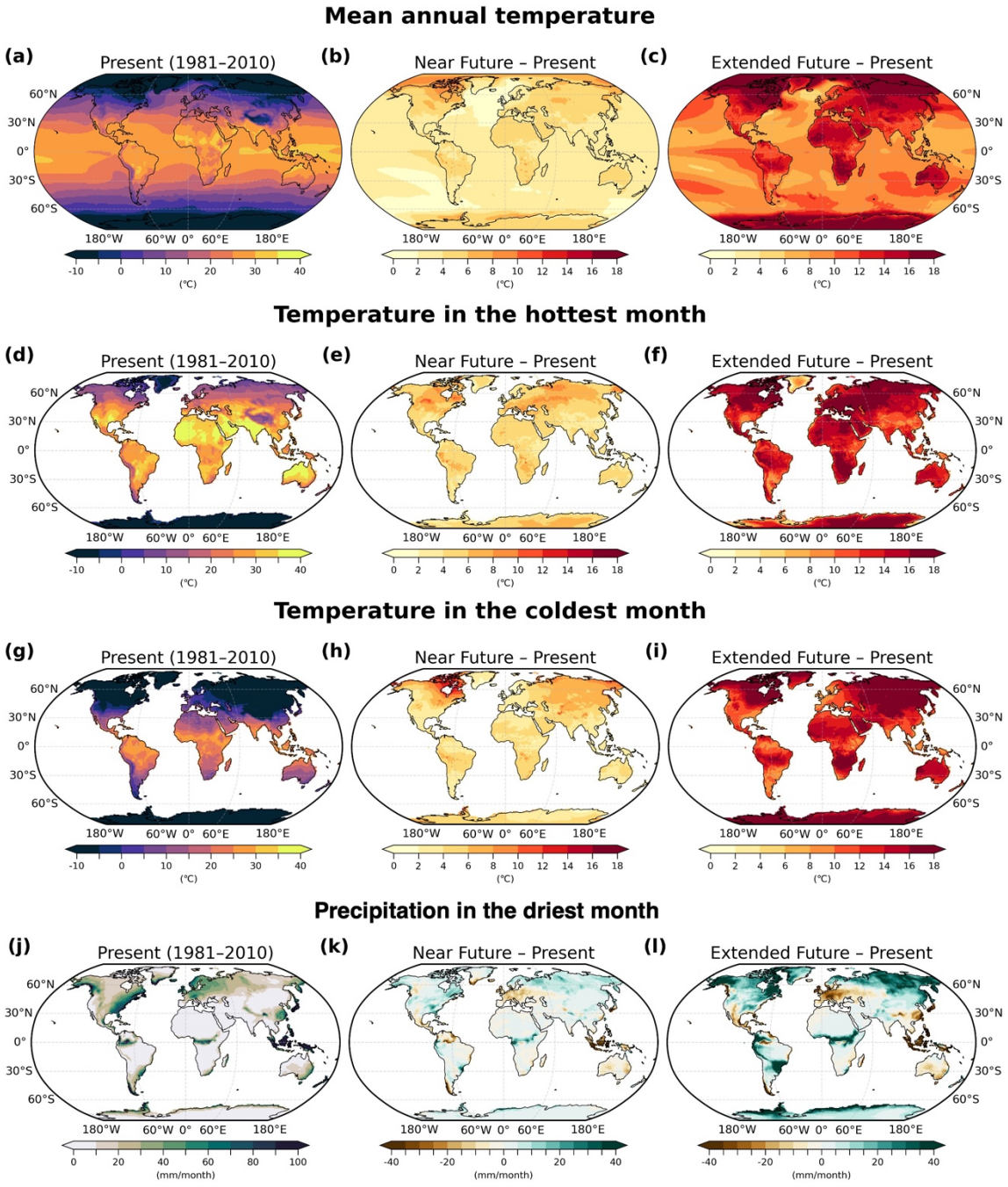

Figure S3. Simulated present-day distributions of key climatic variables and their projected future changes. Rows show (top; a-c) mean annual temperature (°C), (second; d-f) temperature of the hottest month (°C), (third; g-i) temperature of the coldest month (°C), and (bottom; j-l) precipitation of the driest month (mm/month). The left column represents the simulated present-day climatology (1981–2010), while the middle and right columns display projected changes relative to present-day conditions for the near future (2071–2100) and extended future (2271–2300), respectively.

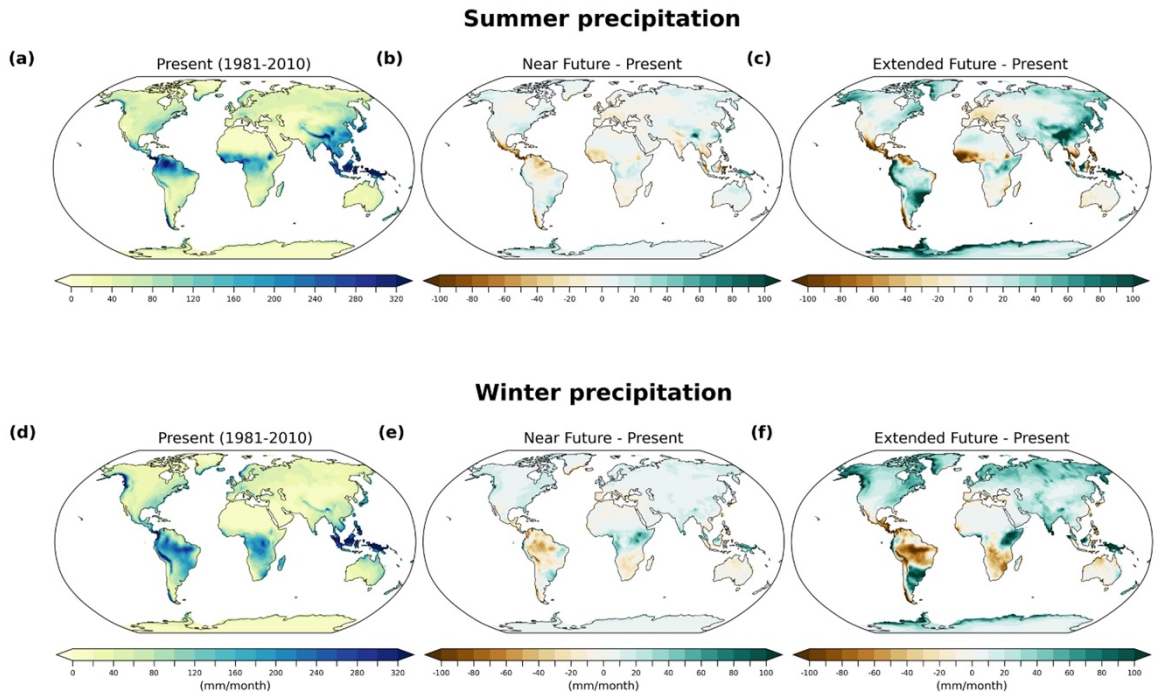

Figure S4. Simulated present-day seasonal precipitation and its projected future changes. Maps display precipitation during (a–c) the summer season (April-September in the Northern Hemisphere and October-March in the Southern Hemisphere) and (d–f) the winter season (October-March in the Northern Hemisphere and April-September in the Southern Hemisphere). The left column presents the present-day climatology (1981–2010), while the middle and right columns show projected changes relative to present-day conditions for the near future (2071–2100) and extended future (2271–2300), respectively.

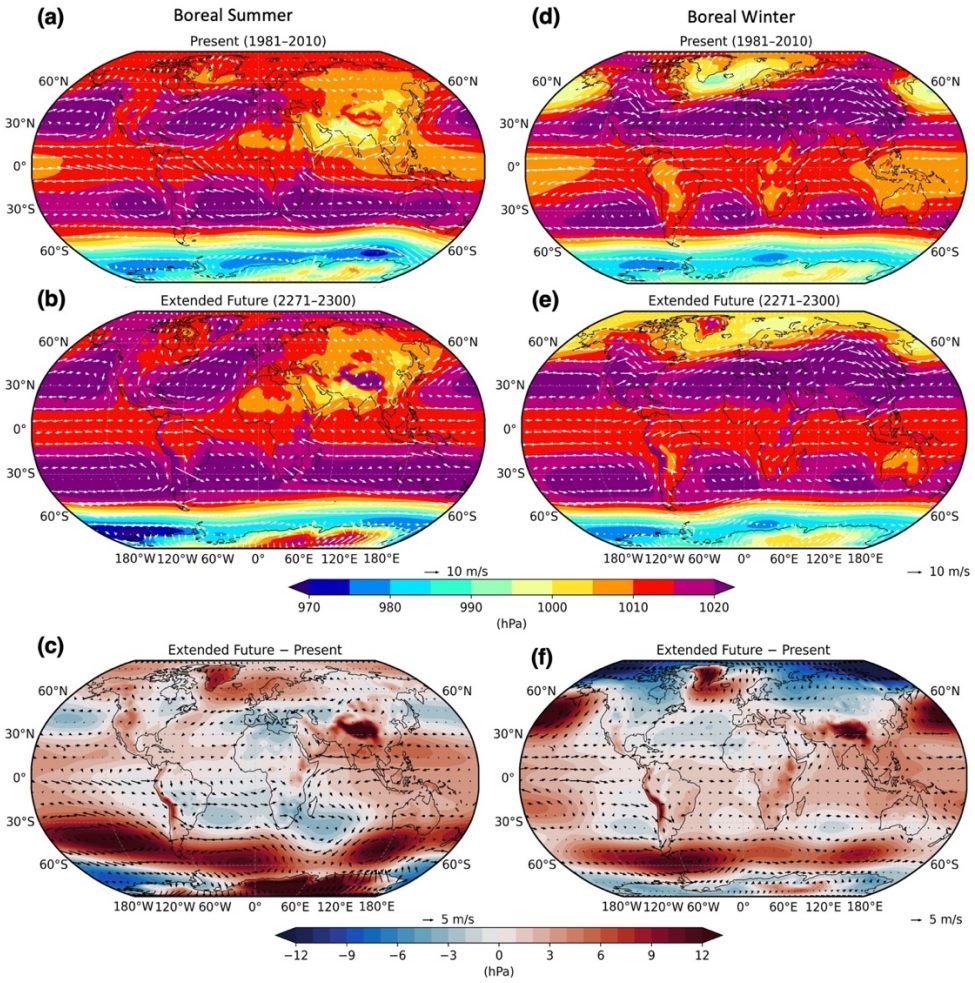

Figure S5. Seasonal sea level pressure and 10-m wind fields for present-day and extended future periods. Shading indicates sea level pressure and vectors denote 10-m winds during (a–c) boreal summer (April-September) and (d–f) boreal winter (October-March). The top and middle rows show climatological means for the present-day period (1981–2010) and the extended future period (2271–2300), respectively. The bottom row displays projected changes (extended future minus present).

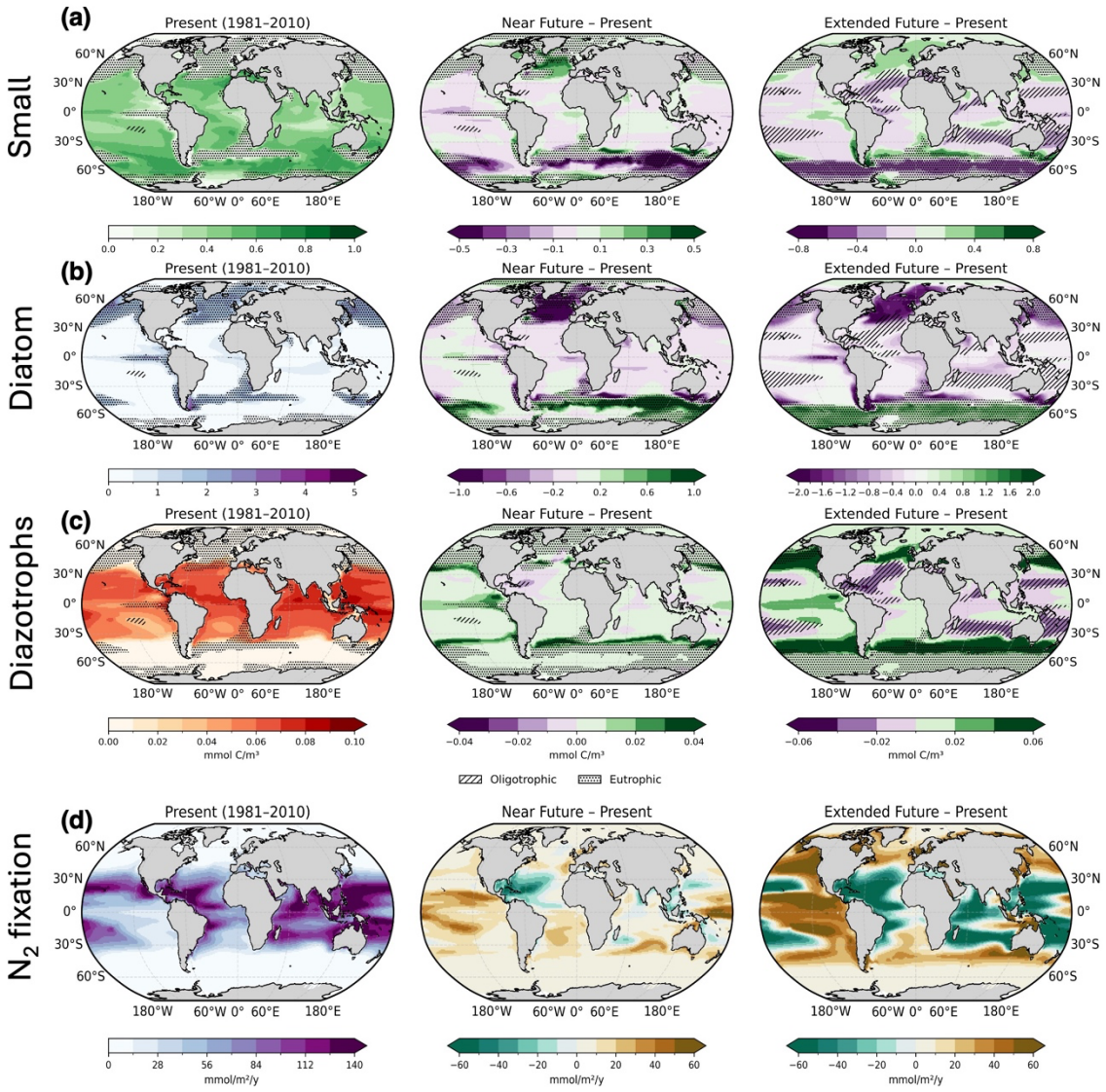

Figure S6. Simulated present-day distributions of phytoplankton biomass and nitrogen fixation, and their projected changes. (a) small phytoplankton biomass (mmol.m^{-3}), (b) diatom biomass (mmol.m^{-3}), (c) diazotroph biomass (mmol.m^{-3}), and (d) nitrogen (N_2) fixation rates (mmol/m^2/year). The left column presents the simulated present-day climatology (1981–2010), while the middle and right columns show projected changes relative to present-day conditions for the near future (2071–2100) and extended future (2271–2300), respectively. Hatched areas in (a–c) indicate regions classified as oligotrophic biomes, and stippled areas indicate eutrophic biomes for each respective period (left: present, middle: near future, right: extended future).

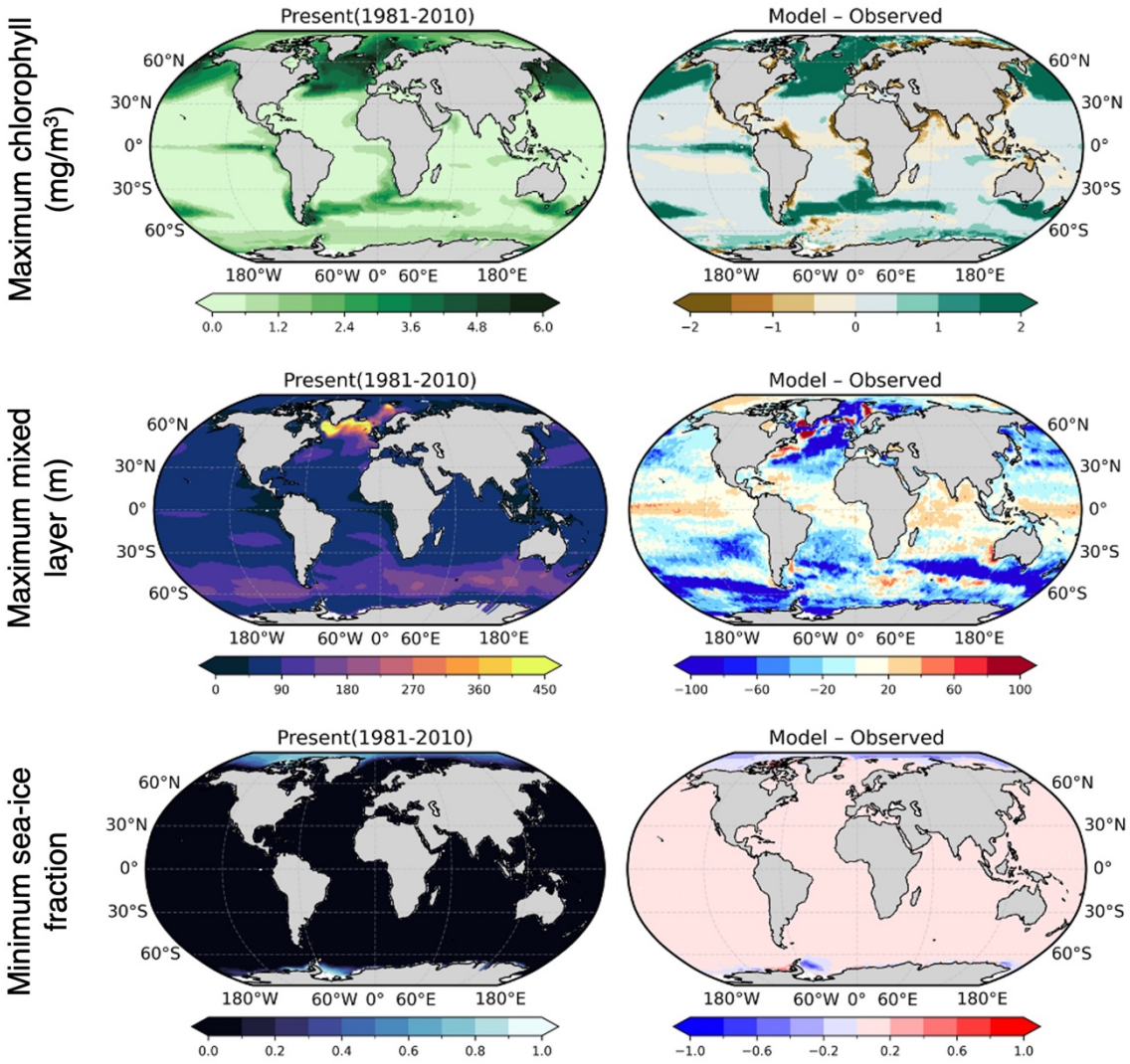

Figure S7. Simulated present-day distributions of key oceanic variables and their comparison with observational climatology. Panels show (top) annual maximum chlorophyll concentration (mg.m-^{3}), (middle) annual maximum mixed-layer depth (m), and (bottom) annual minimum sea-ice fraction. The left column presents the present-day climatology (1981-2010), while the right column represents the model bias relative to observations (model minus observation).

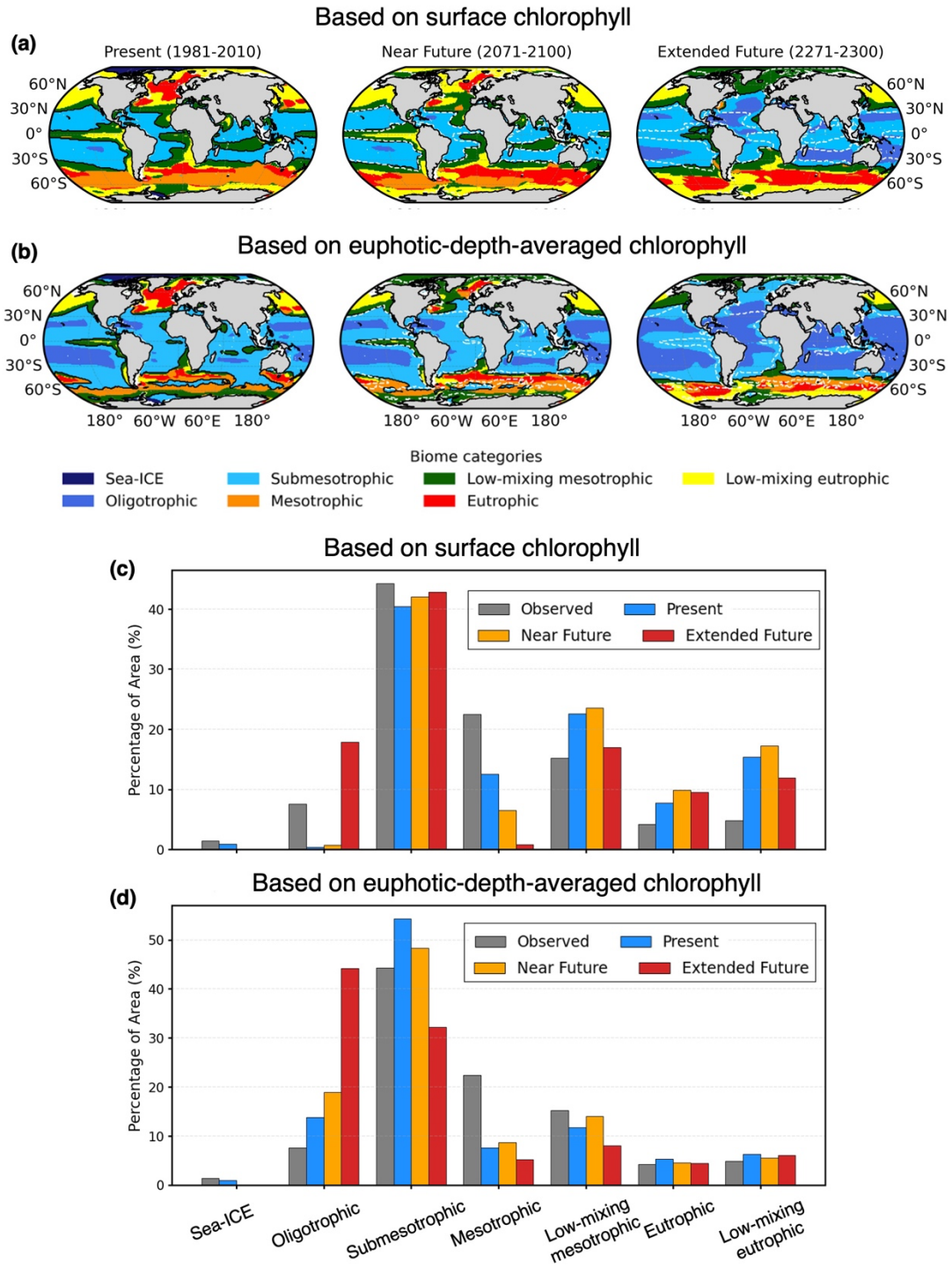

Figure S8. Sensitivity of ocean biome projections to chlorophyll definition. (a, b) simulated ocean biome distributions for the present, near future, and extended future using surface chlorophyll and euphotic-zone-averaged chlorophyll. The white dashed lines in the second and third columns denote the simulated present-day boundary between submesotrophic and mesotrophic biomes, taken from the respective panels in the first column. (c, d) Bar charts of the globally aggregated areas of each ocean biome category under the two chlorophyll definitions.

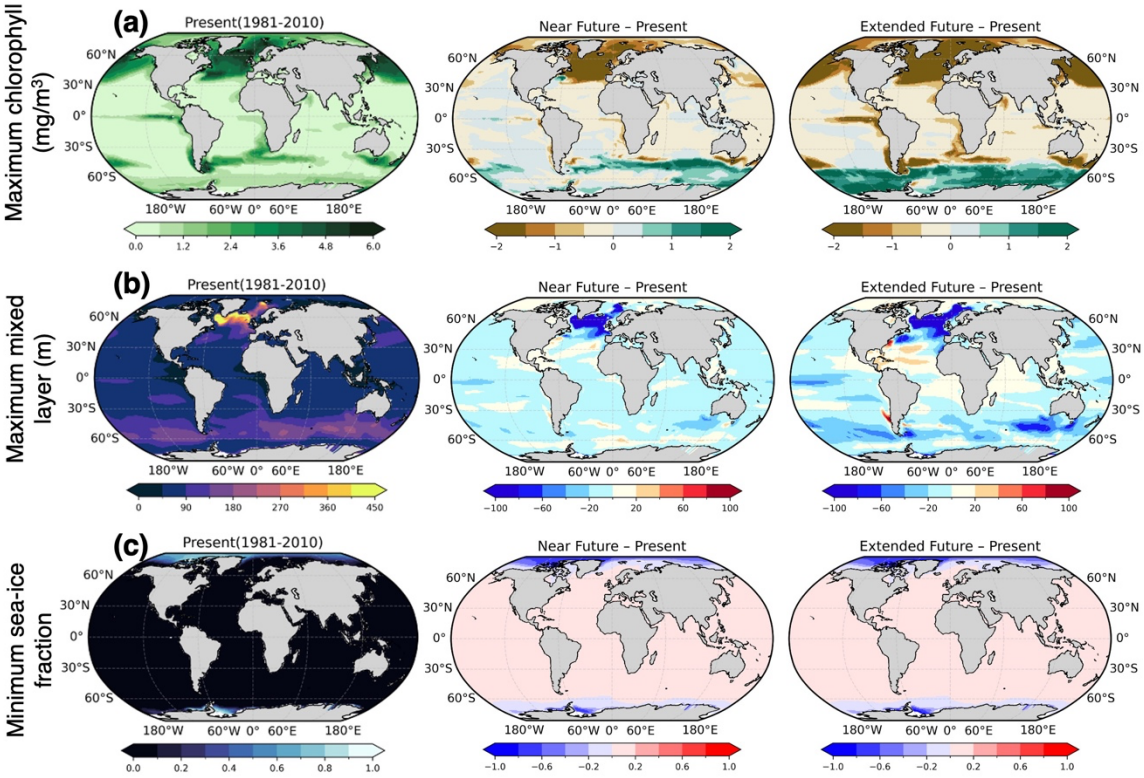

Figure S9. Simulated present-day distributions of oceanic key variables and their projected changes. Panels show (a) annual maximum chlorophyll concentration, (b) annual maximum mixed-layer depth, and (c) annual minimum sea-ice fraction. The left column presents the simulated present-day climatology (1981–2010), while the middle and right columns show projected changes relative to present-day conditions for the near future (2071–2100) and extended future (2271–2300), respectively.

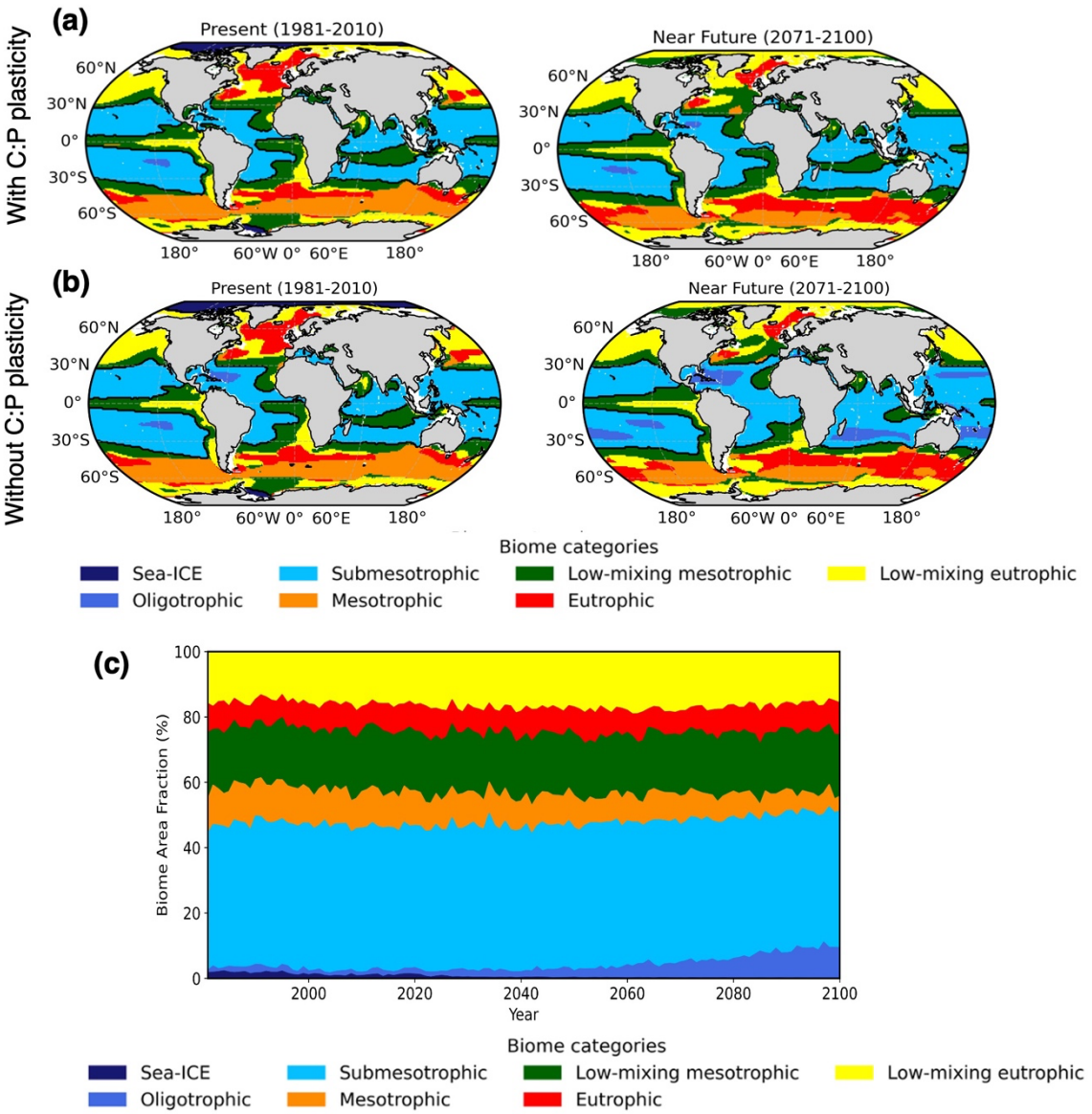

Figure S10. Impact of phytoplankton stoichiometric plasticity on projected ocean biomes. Maps display the spatial distribution of ocean biomes for the present (1981–2010) and near future (2071–2100) simulated under (a) a configuration including C:P stoichiometric plasticity and (b) a configuration without C:P plasticity. (c) Time-series of projected ocean biome area fractions from 1981 to 2100 under a configuration without C:P plasticity.

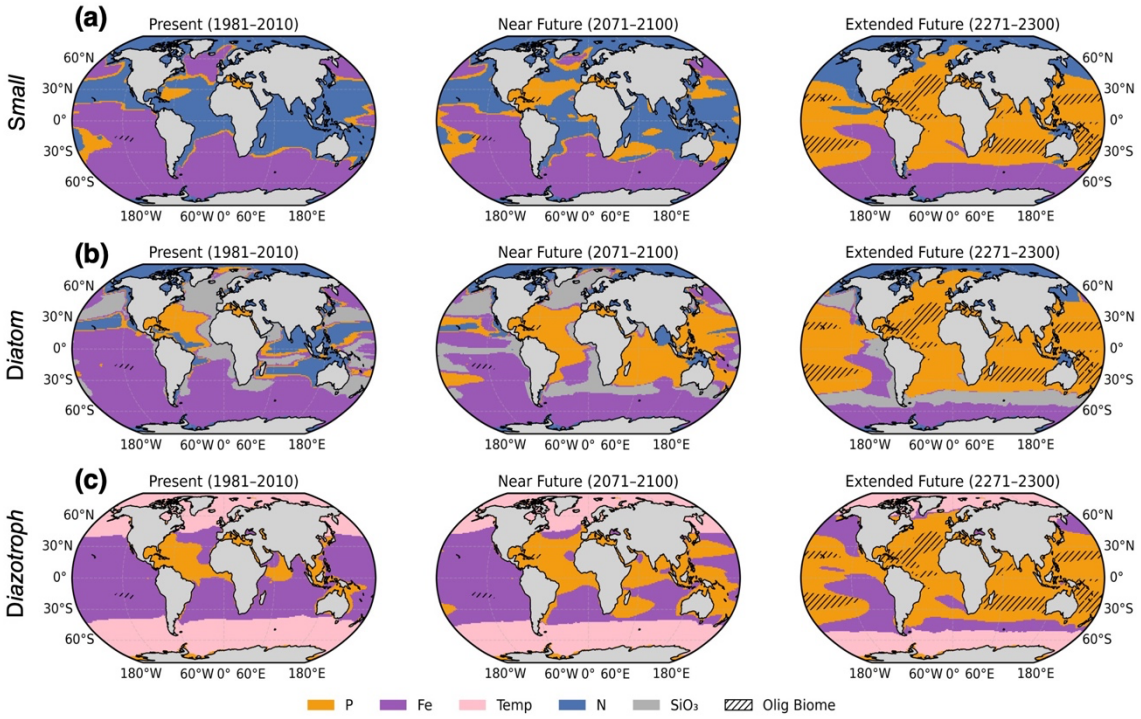

Figure S11. Simulated phytoplankton growth-limiting factors. Maps display the spatial distribution of the primary growth-limiting factor for (a) small phytoplankton, (b) diatoms, and (c) diazotrophs. The columns from left to right represent the present (1981–2010), near future (2071–2100), and extended future (2271–2300) periods. Colors correspond to limitation by phosphorus (P, orange), iron (Fe, purple), temperature (Temp, pink), nitrogen (N, blue), and silicate (SiO_3, grey). Hatched areas indicate the extent of the oligotrophic biome for the respective time period.

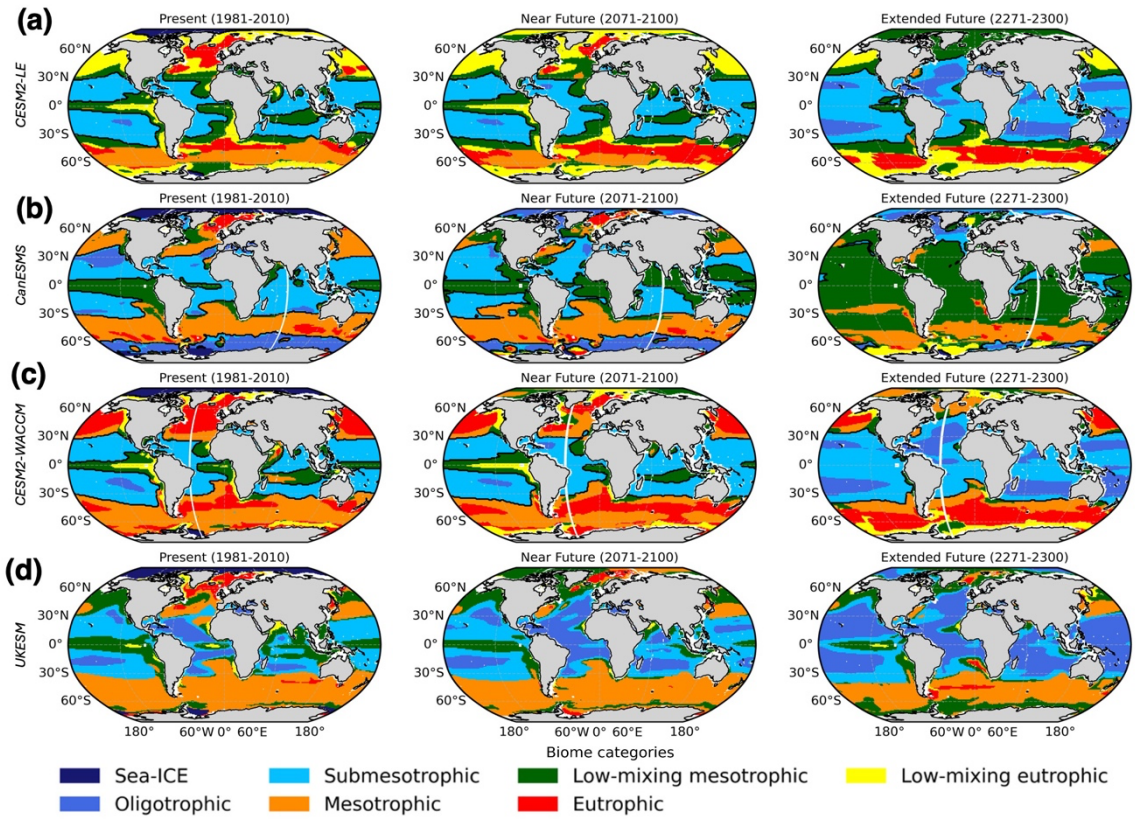

Figure S12. Inter-model comparison of projected marine biome distributions. Maps display the spatial evolution of marine biomes across three scenarios: present (1981–2010), near future (2071–2100), and extended future (2271–2300). The rows represent simulations from four different Earth system models: (a) CESM2-CAM (or CESM2-LE) used in this study, (b) CanESM5, (c)CESM2-WACCM, and (d) UKESM1. The colors correspond to the seven biome categories defined in the legend.